CONF-880260--8

Energy Dependence of Complete and Incomplete Fusion in the $^{28}Si + ^{12}C$ Reaction

CONF-880260--8

DE88 010026

J. F. Mateja
Argonne National Laboratory/Tennessee Technological University
Cookeville, TN 38505

M. F. Vineyard
University of Richmond
Richmond, VA 23173-1903

D. G. Kovar, C. Beck, D. J. Henderson, R. V. F. Janssens, and B. D. Wilkins
Argonne National Laboratory
Argonne, IL 60439

F. W. Prosser
University of Kansas
Lawrence, KS 66044

C. F. Maguire
Vanderbilt University
Nashville, TN 37200

G. S. F. Stephans
Massachusetts Institute of Technology
Cambridge, MA 02139

Time-of-flight (TOF) measurements of the velocity spectra of residues produced in reactions induced by light heavy-ion projectiles ($14 < A < 20$) have shown that at higher bombarding energies ($E_{lab} > 5 - 8$ MeV/nucleon) the velocity centroids are inconsistent, in many cases, with that expected for a complete fusion reaction [1 - 4]. These results have been interpreted as evidence that some fraction of the evaporation residues produced arise from a composite nucleus, formed in a pre-equilibrium or incomplete fusion process, which is moving at a different velocity from that of the complete fusion compound nucleus. A recent study suggests that these incomplete fusion processes depend on the mass asymmetry of the entrance channel [5].

To study possible entrance channel effects in these reactions and to investigate the dependence of such processes on heavier projectiles, measurements involving a pulsed ^{28}Si beam and ^{12}C, ^{28}Si, and ^{40}Ca targets were performed using the ANL ATLAS facility. TOF measurements at ^{28}Si bombarding energies of 11.0, 14.3, and 16.1 MeV/u were carried out to establish the total evaporation residue cross section behavior for complete and incomplete fusion. Reported in this abstract are the preliminary results of the $^{28}Si + ^{12}C$ study.

Two TOF detectors were used to identify the $^{28}Si + ^{12}C$ reaction products. In the first, a microchannel plate detector provided the start signal and a ΔE-E telescope was used to obtain the stop signal (ΔE) and full energy ($\Delta E + E$) of each particle. In the second TOF arm, a ΔE-E telescope was again used to obtain the stop (ΔE) and full energy ($\Delta E + E$)

signals. In this case, however, mass identification was obtained by timing against the pulsed ATLAS beam.

To ensure accurately calibrated energy spectra, each measured fragment energy was corrected event-by-event for energy losses in the target, channel plate foil (in the one time-of-flight arm), gold layers on the fronts of the ΔE and E telescope detectors, and aluminum layer on the back of the ΔE detector. (It should be noted that most of the residues of interest were stopped in the ΔE detector.) In addition, pulse height defect corrections based upon the method of Kaufman were taken into account for each of the Si detectors [6]. Plasma delay corrections which affect the timing signal obtained form Si detectors were also incorporated into the analysis. In this correction, the set of empirical formulae established by Bohne, et al., were used [7].

The velocities of the reaction products were extracted event-by-event using two techniques: 1) by direct time-of-flight measurement corrected for plasma delay, and 2) using the measured energies corrected for pulse height defect and energy losses. Good agreement between the two sets was found.The velocity spectra which were used in the analysis were the ones from the energy measurements.

Reaction products were detected over an angular range from 3^{o} to 20^{o}. The absolute cross section was obtained by normalizing the elastic scattering data with the results of an optical model calculation using the $^{28}Si + ^{12}C$ parameter set H12 of DeVries [8].

The velocity spectrum for each residue mass ($12 \leq A \leq 39$) was individually inspected to determine the magnitudes of the complete and incomplete fusion components and to identify any yield which might arise from competing reaction processes. The non-evaporation component, found primarily within three mass units of the projectile mass, was readily identifiable as it had a near-projectile velocity. The velocity centroids for the fusion-evaporation events, on the other hand, were approximately one half that of the beam velocity. Further, the magnitude of the non-fusion component fell very rapidly with angle, in most cases exhausting its strength by 8^{o}-10^{o}. The fusion-evaporation component extended out to about 20^{o}.

The complete fusion component of the evaporation residues was determined by a comparison of the experimental velocity spectra with the velocity spectra predicted by the Monte-Carlo Evaporation Code LILITA [9]. The maximum yield consistent with complete fusion was determined by normalizing the magnitude of the predicted velocity distribution to the distribution observed for each mass at each angle. Held fixed in this analysis was the width and position of the predicted velocity distribution. This procedure is believed to provide a limit on the maximum possible complete fusion cross section.

The summed angular distributions ($12 \leq A \leq 39$) for the complete fusion yield (dashed curve) and the total evaporation residue yield (incomplete + complete - solid curve) for the 14.3 MeV/u data are presented in Fig. 1. The integrated cross sections, found by using a smooth extrapolation between data points, for all bombarding energies studied in this experiment are presented in Table I as Decomposition 1.

The dotted curve in the Fig. 1 is the complete fusion angular distribution predicted by LILITA. As can be seen, the calculated angular distribution is narrower than that associated with the yields identified in our velocity decomposition as consistent with complete fusion evaporation residues. In an attempt to understand the origin of the enhanced back-angle yield in the experimental angular distributions, the angular distributions of the individual mass residues were studied. We found that the heavy residue masses ($A > 24$) were well predicted by the LILITA calculation over the entire angular range. The experimental angular distributions for the lighter residues (A < 22), however, were substantially broader than those predicted by LILITA. This is illustrated in Fig. 2. The origin of this broadening is not fully understood at present. It is not clear whether the result is attributable to the inadequacies of the LILITA calculations, not including for example the emission of heavy particles like ^{8}Be, or whether there has been a misidentification of fusion events. An integration of the LILITA angular distributions (normalized to the data at forward angles) was performed to provide an estimate of the complete fusion cross section in the event that the back-angle broadening arises from some reaction process other than fusion (see Table I, Decomposition 2).

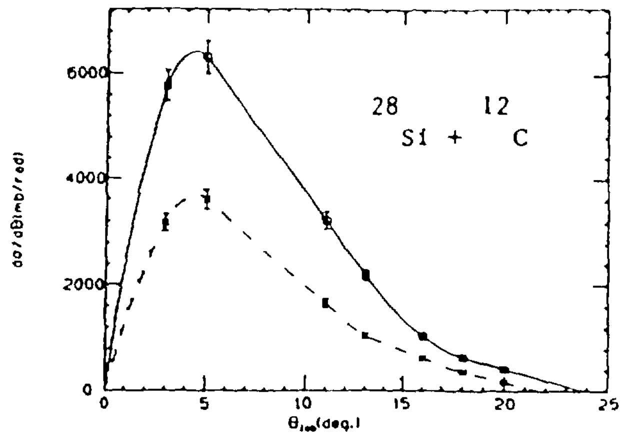

Fig. 1. Angular distribution of the total evaporation residues (solid), complete fusion (dashed), and LILITA (dotted) at 14.3 MeV/u.

Our integrated cross sections have been included in the $1/E_{c.m.}$ plot presented in Fig. 3. The results are shown as bars, the lower limit corresponding to the value obtained by following the LILITA angular distribution and the upper limit by following the extracted experimental points. As can be seen in the figure, our results are in good agreement with the theoretical predictions of Frobrich [10]. We are, however, in poor agreement with the trend in the data suggested by the recent study of Harmon et al. [11]. As can be seen in Fig. 3, Harmon's results are not in agreement with an earlier experimental study.

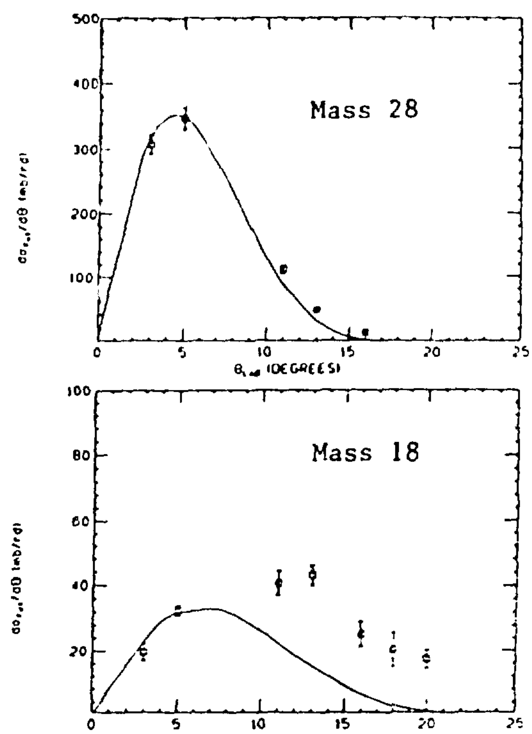

Fig. 2. Angular distributions for the complete fusion yields of masses 28 and 18. The solid curves are the LILITA predictions.

Finally, the ratio of complete fusion to total evaporation residue cross section shown in Fig. 4, are consistent with the Morgenstern systematics which argue for an entrance channel mass asymmetry dependence of the incomplete fusion process. However, it should be noted that the procedure used to identify the complete fusion yield can only provide an upper limit on the cross section, and if significant pre-equilibrium single or two nucleon emission is present our procedure will over estimate the cross section.

Work supported by the U.S. Department of Energy, Nuclear Physics Division, under Contract W-31-109-ENG-38.

Table I. $^{28}Si + ^{12}C$ integrated cross sections.

Energy MeV/u	Evaporation Residues (complete + incomplete) mb	Complete Fusion Decomp 1[a] mb	Decomp2[b]
11.0	1222	772	722
14.3	1100	597	497
16.1	1171	537	414

[a] Decomposition consistent with the experimental velocity distribution.

[b] Decomposition consistent with the experimental velocity distribution and the angular distribution predicted by LILITA.

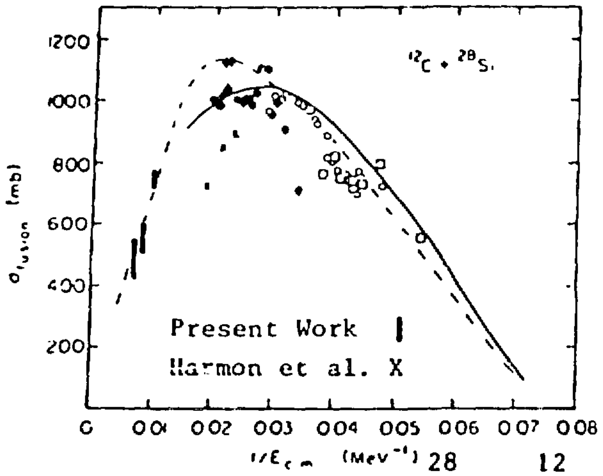

Fig. 3. $1/E_{c.m.}$ plot for $^{28}Si + ^{12}C$ taken from Ref. 10. The solid curve is the theoretical prediction of Frobrich.

1. H. Morgenstern, et al., Phys. Lett. 113B, 463 (1982).
2. Y. Chan, et al., Phys. Rev. C27, 447 (1983).
3. T. Humanic, et al., Bull. Am. Phys. Soc. 27, 478 (1982).
4. H. Morgenstern, et al., Z. Phys. A313, 39 (1983).
5. H. Morgenstern, et al., Phys. Rev. Lett. 52, 1104 (1984).
6. S. B. Kaufman, et al., Nucl. Inst. Meth. 115, 47 (1974).
7. W. Bohne, et al., Nucl. Inst. Meth. A240, (1985).
8. R. M. DeVries, et al., Phys. Rev. Letts. 39, 450 (1977).
9. J. Gomez del Campo and R. Stokstad, Private Communication.
10. P. Frobrich, Phys. Rep. 116, (1984).
11. B. A. Harmon, et al., Phys. Rev. C34, 552 (1986).

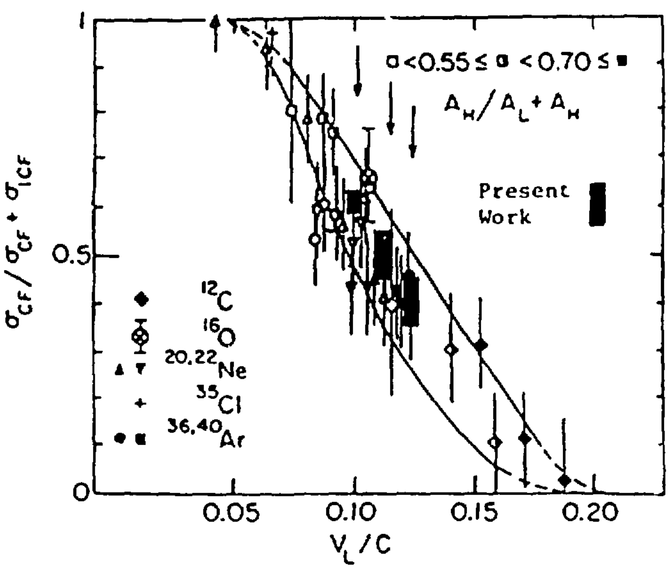

Fig. 4. Figure from Ref. 5 displaying the fraction of complete fusion evaporation residue yield as a function of the velocity of the lighter nucleus v_1/c.

DISCLAIMER